Fourier-based Radar Processing for Multistatic Millimetre-wave Imaging with Sparse Apertures

Vasiliki Skouroliakou, Amir Masoud Molaei, Vincent Fusco, Okan Yurduseven
Institute of Electronics, Communications and Information Technology (ECIT), Queen's University Belfast, Belfast BT3 9DT, United Kingdom
vskouroliakou01@qub.ac.uk; a.molaei@qub.ac.uk; v.fusco@ecit.qub.ac.uk; okan.yurduseven@qub.ac.uk

***Abstract*—Fourier-based radar processing algorithms have attracted a lot of interest among imaging techniques mostly because they are extremely fast. Moreover, such techniques can be integrated with a Multiple-Input Multiple-Output (MIMO) effective aperture, able to alleviate the hardware constraints, to form a cost-effective imaging system that can retrieve an estimation of the scene in real-time. The proposed technique leverages the phase center approximation and a multistatic-to-monostatic data conversion to render the back-scattered measurements compatible with fast Fourier processing. Whereas the phase center approximation is applicable for imaging in the far-field of the synthesized aperture, in the near-field, a more sophisticated aperture design should be considered to reduce the distortion in the reconstructed images. This paper presents a theoretical study for a sparse aperture design and the optimization of the aperture layout in the context of the phase center approximation validity for near-field imaging facilitated by Fourier-based reconstructions. Furthermore, it proposes a GPU accelerated reconstruction algorithm able to form 3D images in a few milliseconds with low-cost hardware.**

***Index Terms*—millimeter-wave imaging, three-dimensional imaging, Fourier-based image processing, MIMO sparse aperture, near-field imaging**

I. Introduction

Millimeter-wave imaging is gaining significant popularity among a variety of applications, with surveillance systems and detection of concealed items being some of the most noteworthy examples. Particularly in the context of security-screening, the superiority of such a system lies in a variety of reasons, such as the capability of millimeter-waves to penetrate common clothing and other optically opaque materials to form an image of a person carrying any concealed items. Moreover, radiation at millimeter-wave frequencies is non-ionizing, hence, does not pose any health hazards. Millimetre-wave imaging can also achieve a high resolution due to the relatively short wavelength (1-10 mm) at these frequencies.

Traditionally, millimeter-waver imaging systems rely on Synthetic Aperture Radar (SAR) technology [1-3] to mechanically scan the target scene satisfying Nyquist criteria. However, this configuration, although associated with high quality images, requires a large number of channels and considerable amount of time to acquire the back-scattered information. Nevertheless, since the measurements on the aperture side are derived from a point-by-point raster scanning, they are uniformly sampled, and thus can be handled using Fourier-based processing techniques [1], addressing the image reconstruction problem in real-time.

To alleviate the above constraints, computational imaging approaches have been used in the literature [4-7]. However, such configurations demand the inversion of an ill-posed matrix, which results in a bottleneck in achieving fast image reconstruction time. Alternatively, a compressed sensing approach via an effective aperture [8-12] could also meet the hardware constraints, reducing significantly the number of elements and thus the acquisition time and the cost of the system.

Although meeting the hardware constraints, the above configurations transfer the complexity from the acquisition step to the signal processing step. Since fast reconstruction is essential for real-time applications, image processing in the frequency domain, utilizing Fourier transformations, is preferable over computational techniques in spatial domain. A traditional Fourier-based reconstruction algorithm, like the one demonstrated in [1] for a monostatic aperture, will not be sufficient in multistatic configurations, since the data are not derived from a point-by-point scanning of the target scene. Hence, more sophisticated image reconstruction techniques need to be developed that usually involve pre-processing steps. In this paper, we present the aperture design constraints for Fourier-based image reconstruction in MIMO radars with sparse apertures as applied to near-field imaging problems at millimeter-wave frequencies.

The rest of the paper is organized as follows: Section II analyses the proposed Fourier-based technique for multistatic apertures leveraging the effective aperture concept, Section III discusses the importance of a more sophisticated aperture design in near-field and supports the hypothesis with simulation results, Section IV refers to the algorithm implementation and performance and lastly Section V includes the conclusions.

II. Image Reconstruction Technique

A. Fourier-based Imaging

Fourier-based reconstruction techniques are very appealing since they can be implemented leveraging the Fast Fourier Transform (FFT) algorithm, which is known for its high computational efficiency. Naturally, to take advantage of the FFT, the data need to be uniformly sampled. This is usually

the case in monostatic imaging configurations [1], where a co-located transmitter-receiver source is scanned, mechanically or electronically to form the whole aperture. At the end of the raster scan, the collected information will be uniformly sampled and readily compatible with fast Fourier processing.

An estimation of the scene can then be retrieved using the following equation [1]:

$$f(x,y,k) = IFFT_{2D}[FFT_{2D}[s(x,y,k)e^{-j\sqrt{4k^2-k_x^2-k_y^2}z_0}]] \quad (1)$$

In the above equation, $s(x,y,k)$ represents the back-scattered signal recorded by the transceiver. The signal is evaluated at multiple frequencies and $k = 2\pi f/c$, where c stands for the speed of light in vacuum, symbolizes the corresponding wavenumber. The exponential term stands for the dispersion relation [1]. The abbreviation IFFT denotes the Inverse Fast Fourier Transform (IFFT). After the IFFT, the third dimension is coherently summed to obtain a two-dimensional (2D) image plane f(x,y), which is an estimation of the imaged scene. For three-dimensional (3D) imaging multiple image planes are considered at different range distances z_0 from the aperture. All the planes are finally combined to obtain one 3D image.

B. Multistatic Fourier-based Imaging

1) The multistatic aperture: Although monostatic imaging seems very attractive due to the direct compatibility with FFT techniques, the substantial amount of acquisition time and number of channels associated with it hinders its use in practical applications.

On the other hand, multistatic apertures promise to alleviate the above restrictions, leading to a more effective imaging system. Multistatic imaging benefits from the effective aperture concept [9-11], according to which N_{R_X} receiving elements and N_{T_X} transmitting elements can form up to $N_{R_X}N_{T_X}$ spatially diverse positions. Consequently, the effective aperture concept eliminates the need for physically densely sampled apertures on the condition that the synthesized effective aperture provides sufficient sampling. In other words, the number of transmit and receive antennas can be substantially reduced, resulting in a sparse aperture layout.

A typical sparse MIMO 2D aperture is depicted in Fig. 1(a) [9,11]. The aperture is divided into multiple clusters, each of them looks like the one in Fig. 1(b). More details about the need of clustering are mentioned in the next section. As depicted in Fig. 1(b) each cluster consists of receiving elements, which are represented by red dots along the x-axis, and transmitting elements which are represented by blue dots along the y-axis. The element spacing is subject to λ_{min}, which is the wavelength corresponding to the maximum frequency of the band. Each transmitting antenna propagates millimeter-waves to the scene and each receiving antenna within the same cluster records the back-scattered information.

The multistatic back-scattered measurements will then be in the form $s(x_T, y_T, x_R, y_R, k)$, i.e, they are a function of the position of each transmitting and receiving antenna and each

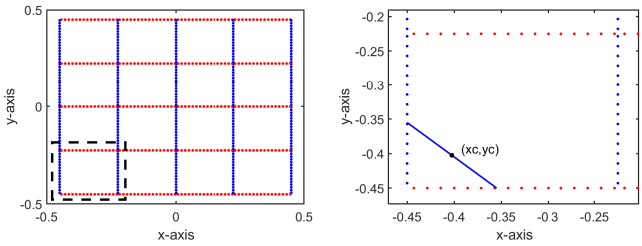

(a) (b)

Fig. 1: (a) A 2D sparse MIMO aperture of size D=0.9m. The receiving elements are represented with red dots, while the transmitting with blue. (b) One cluster of size D'=0.225m highlighted with the dashed rectangle in Fig. 1(a).

frequency point in the band. Thus, they cannot be used as they are in (1).

2) The phase center approximation: In Fig. 1(b), one cluster of the aperture in Fig. 1(a) is depicted. In case that the length of each cluster is small enough compared to the imaging distance, the distance between each transmitter-receiver pair within the same cluster will also be small compared to the imaging distance. Therefore, we can assume that the target is in the far-field in terms of each cluster. Thus, an effective phase center can be formed between each transmitter-receiver pair within the same cluster [11-12]. In Fig. 1(b) one such phase-center is shown, formed by a random transmitter-receiver pair. Physically, the phase-center lies in the middle of the distance between them, therefore letting (x_T, y_T) and (x_R, y_R) be coordinates of the antenna elements pair, the coordinates of their phase center are,

$$x_c = \frac{x_R + x_T}{2} \quad , \quad y_c = \frac{y_R + y_T}{2} \quad (2)$$

The process of forming a phase-center is repeated for every transmitting-receiving pair within each cluster, such that a grid of phase centers is created that covers the whole surface of the aperture. This grid is uniform and is spaced by $0.5\lambda_{min}$, resembling the grid of a monostatic aperture. If we could transform the back-scattered measurements of the multistatic aperture, such that they are sampled on this phase centers grid, we will be able to reconstruct the scene using (1).

3) Multistatic-to-monostatic conversion: The answer to the above speculation has been given in the literature developing a multistatic-to-monostatic conversion of the back-scattered measurement set, [11-12]. A reference point is defined to establish this conversion. This point lies on the center of the imaging scene, and its coordinates are $x_{ref}, y_{ref}, z_{ref}$. Then the multistatic back-scattered set $s(x_T, y_T, x_R, y_R, k)$ will be transformed to a monostatic one $\hat{s}(x_c, y_c, k)$ through the following relationship:

$$\hat{s}(x_c, y_c, k) = s(x_T, y_T, x_R, y_R, k)\frac{\hat{s}_{ref}(x_c, y_c, k)}{s_{ref}(x_T, y_T, x_R, y_R, k)} \quad (3)$$

where $\hat{s_{ref}}$ stands for the back-scattered signal of a hypothetical monostatic aperture imaging the scene consisting only of the reference point, and accordingly, s_{ref} stands for the the back-scattered signal of the multistatic aperture imaging the scene consisting only of the reference point. The reference signals are

$$\begin{aligned} s_{ref}(x_T, y_T, x_R, y_R, k) &= e^{-jk(R_T+R_R)} \\ \hat{s}_{ref}(x_c, y_c, k) &= e^{-2jkR_c} \end{aligned} \tag{4}$$

where R_T and R_R stand for the distances between the reference point and each transmitter and receiver in the multistatic array, respectively. In the monostatic scenario, R_c symbolizes the distance between the co-located antenna and the reference point. Assuming that the center of the imaging scene, i.e. the reference point, is the point with coordinates $(0, 0, z_0)$, the distances are defined as follows:

$$\begin{aligned} R_T &= \sqrt{{x_T}^2 + {y_T}^2 + {z_0}^2} \\ R_R &= \sqrt{{x_R}^2 + {y_R}^2 + {z_0}^2} \\ R_c &= \sqrt{{x_c}^2 + {y_c}^2 + {z_0}^2} \end{aligned} \tag{5}$$

After the transformation in (3), we can use (1) to retrieve an estimation of the target scene.

III. Near-field imaging

The effective aperture concept described in Section II is strictly valid in the far-field of the aperture [10]. This assumption becomes less accurate as the imaged object is located closer to the aperture, extending into the near-field region. Hence, for near-field applications a more sophisticated design of the aperture should be considered to avoid the distortion in the final image. The minimum far-field distance is subject to:

$$d_{far\_field} = \frac{2D^2}{\lambda} \tag{6}$$

where λ is equal to λ_{min} and D is the size of the aperture in meters. Strictly speaking, to achieve a non-distorted image an imaging distance at least equal to the one given by (6) is required.

By clustering the aperture as shown in Fig. 1(a) and ensuring that no cross-cluster interactions occur, it is possible to measure the far-field distance in terms of the size of each cluster and not of the whole aperture. As a result, the phase center approximation can hold accurate within each cluster without the necessity of the overall physical aperture to satisfy the far-field condition.

It is important to clarify at this point that the purpose of using the proposed method is to minimize the distortion caused by the violation of the far-field condition and not to vanish it. In other words, one can continue increasing the number of clusters within the aperture until each cluster is small enough such the target scene is strictly in the far-field of each cluster. However, this increases the physical layer complexity due to having an unfeasible number of clusters. Evidently, there is a trade-off between the number of clusters the aperture can be partitioned into, hence the system complexity, and the corresponding far-field distance for each cluster to satisfy the phase center approximation. Our goal in this paper is to find an optimal solution to this trade-off. As part of this study, we will show through simulations that satisfying results could be achieved even though the far-field condition is not strictly satisfied while keeping the number of clusters at an acceptable level.

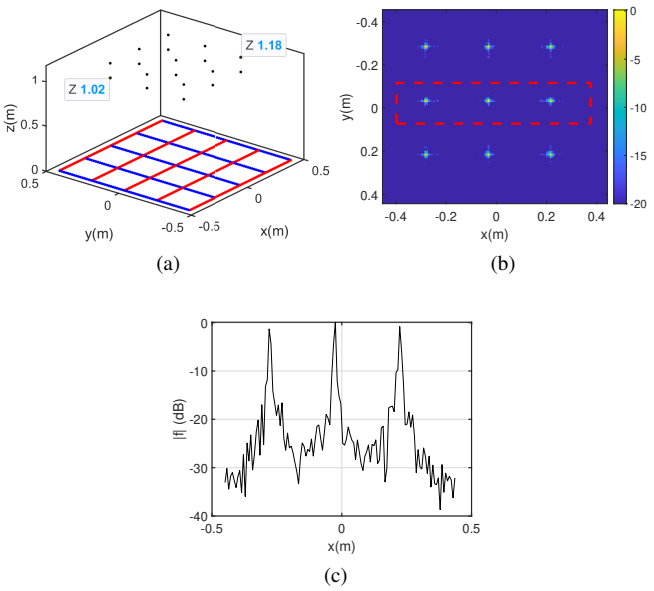

Fig. 2: (a) The sparse MIMO aperture consisting of 16 clusters and target scene. (b) The cross-range plane. (c) Cross-range resolution curve.

In the configuration depicted in Fig. 1(b), in each cluster 16 receiving elements are considered along the top and bottom boundaries and 16 transmitting elements along the lateral boundaries. The element spacing is subject to λ_{min}. We use a 2GHz bandwidth (B) in K-band, from 19GHz to 21GHz and thus λ_{min}=14.3mm. Consequently, using the effective aperture principle, $32 \times 32 = 1024$ phase centers are created within each cluster and $16 \times 1024 = 16384$ within the whole surface of the aperture. The size of each cluster is equal to D' = 0.225m. Hence, according to (6), the far-field distance will be equal to 7.1m. We consider an imaging distance equal to 1m, which is comparable to the distance of the far-field limit. The target scene consists of two sets of nine point scatterers lying on different depth distances, as shown in Fig. 2(a). The results are illustrated in Fig. 2.

We focus in the cross-range plane (xy) and cross-range resolution here, since the range plane (z) is mostly affected by the bandwidth. The cross-range plane is depicted in Fig. 2(b), expressed in dB scale. We observe that all point scatterers are resolved and almost no distortion is detected in the reconstructed image. In Fig. 2(c) the cross-range curves for a specific horizontal point, as indicated by the rectangle in Fig. 2(b), are shown.

We repeat the experiment employing an aperture of the same

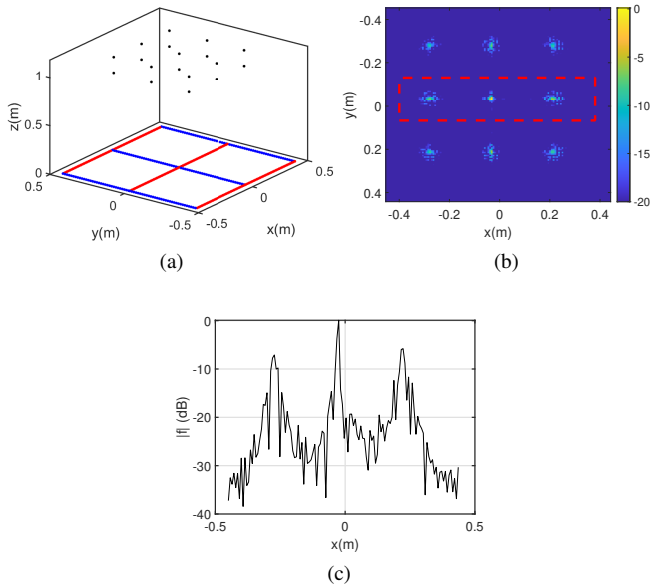

Fig. 3: (a) The sparse MIMO aperture consisting of 4 clusters and target scene. (b) The cross-range plane. (c) Cross-range resolution curve.

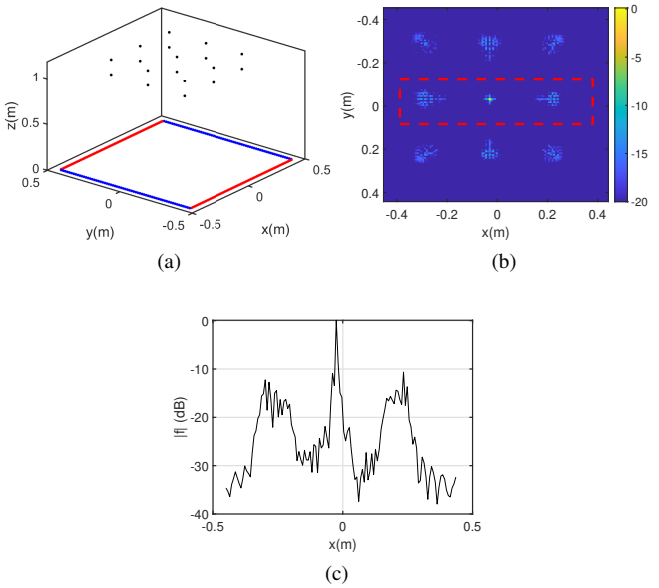

Fig. 4: (a) The sparse MIMO aperture consisting of a single cluster and the target scene. (b) The cross-range plane. (c) Cross-ranger resolution curve.

size but now divided into four clusters, each one of size D' = 0.45m, as shown in Fig. 3(a). The far-field limit is now equal to 28.3m. In this case, the limit significantly exceeds the near-field target distance of 1m, hence, we expect to observe a noticeable violation of the phase center approximation, resulting in an increased distortion in the final image. The results shown in Fig. 3 confirm this observation.

Lastly, we consider an aperture consisting of a single cluster of size D'= 0.9m, as shown in Fig. 4(a). The far-field distance is now equal to 113.3m. The results are demonstrated in Fig. 4. In this case, the simple aperture layout consisting of a single cluster is achieved at the cost of significantly violating the phase center approximation, resulting in a heavily distorted reconstruction.

It is evident that in Fig. 3(b) and Fig. 4(b) the corner point scatterers experience a greater amount of distortion. The distortion gets significantly worse in Fig. 4(b). This phenomenon becomes more apparent when looking at the resolution curves in Fig. 3(c) and Fig. 4(c). The resolution curve for the corner points does not have a clear peak point and it is affected a lot by the side lobes. This is an expected outcome derived from the paraxial approximation holding true within small angle variations around the optical axis [8]. In close range, the variations become more significant and thus the points that are away from the optical axis, i.e., the corner ones, are mostly affected.

In Fig. 5(a), the Normalized Mean Squared Error (NMSE) is illustrated for all above configurations as a function of the number of clusters. The NMSE is subject to the formula [15]:

$$NMSE = \frac{\sum |f_{est} - f|^2}{\sum |f|^2} \tag{7}$$

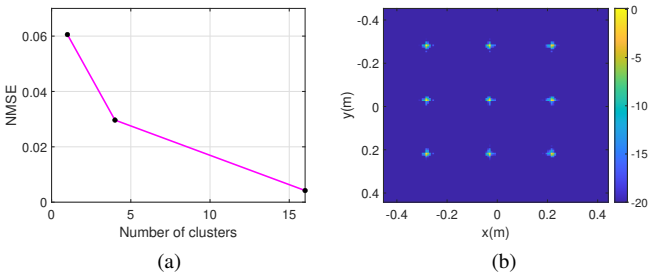

Fig. 5: (a) The NMSE of the above reconstructed cross-range planes as a function of the number of clusters. (b) The cross-range plane of a configuration involving 64 clusters. Considered ideal condition here.

The ideal condition is considered the case of 64 clusters, which brings each cluster even closer to the far-field limit. The cross-range plane for this scenario is shown in Fig. 5(b). Observing Fig. 5, it is clear that increasing the number of clusters in the aperture beyond this limit will not lead to any significant improvement in the cross-range of the final image.

IV. Algorithm Implementation

The algorithm addressing the image reconstruction for all the configurations discussed above was developed on a single GPU using C language and CUDA programming. The GPU card is a NVIDIA Tesla M60 with 16GB of memory.

The algorithm was developed considering a 3D scene, as illustrated in Fig. 2(a). The scene is of the same size with the aperture in cross-range and half this size in depth. Hence, it is equal to $0.9m \times 0.9m \times 0.45m$. To determine the number of

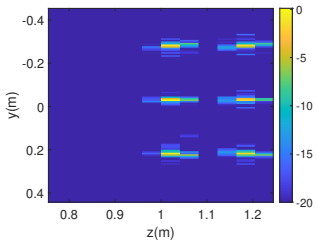

Fig. 6: The range plane for 16 clusters and B=2GHz.

depth slices, the scene's depth is divided with the theoretical range resolution in near-field, given by the formula [14]:

$$\delta_r = \frac{c}{2}(B + f_{min}(1 - \frac{1}{\sqrt{(1 + (\frac{D}{2z_0})^2)}}))^{-1} \quad (8)$$

In this case, the range resolution is equal to 40mm and 12 range slices are considered.

The input matrix to the reconstruction function is a 3D matrix $s(x, y, k)$, according to (1). For this implementation, its dimensions are $128 \times 128 \times 32$, where 32 stands for the number of frequency samples within the band. This matrix is translated for all range slices. After the reconstruction process is completed for a slice, we sum the third dimension to obtain o 2D plane. Finally, all 2D planes are combined to obtain one 3D image of size $128 \times 128 \times 12$.

The range plane, derived from the physical setup shown in Fig. 2(a), is shown in Fig. 6 for 16 clusters. The middle targets located at two different range distances as shown in Fig. 2(a), are depicted. We can observe that the algorithm is able to locate the targets properly in the range plane.

The total execution time (including data transfers to and from the GPU) of the reconstruction algorithm is equal to 21ms, considering the first scenario with 16 clusters. A traditional back-projection algorithm [13] needs about 11.6h to be executed on CPU, while the proposed approach is executed in 100ms on CPU. Consequently, the GPU implementation offers a speedup equal to $1.6e^6$ and 4.8 against the first and the latter implementation, respectively. It is evident that the FFT-IFFT approach supported with the GPU acceleration constitutes a significant step towards real-time operation.

V. Conclusions

This paper presents a Fourier-based imaging technique suitable for MIMO apertures. We argued, and supported by simulation results, that a more sophisticated aperture design should be considered in near-field to alleviate the distortion in cross-range plane reconstruction. The proposed technique is shown to produce high fidelity results in the range plane as well. Lastly, we argued that fast execution time can be achieved for the reconstruction process, i.e., in the order of a few milliseconds, by utilizing GPU acceleration. This is a promising result concerning the execution time of the algorithm in more practical scenarios, particularly for an application requiring real-time operation.

Acknowledgment

This work was funded by the Leverhulme Trust under Research Leadership Award RL-2019-019.

References

[1] D. M. Sheen, D. L. McMakin, and T. E. Hall, "Three-dimensional millimeter-wave imaging for concealed weapon detection," IEEE Transactions on microwave theory and techniques, 49(9), 1581-1592, 2001.

[2] A. Moreira et al., "A tutorial on synthetic aperture radar," IEEE Geoscience and remote sensing magazine, 1(1), 6-43.

[3] A. W. Doerry, and F. M. Dickey, "Synthetic aperture radar," Optics and photonics news, 15(11), 28-33, 2004.

[4] W. Li, J. Qi, and A. Sihvola, "Meta-Imaging: from Non-Computational to Computational," Advanced Optical Materials, 8(23), 2001000, 2020.

[5] J. N. Mait, G. W. Euliss, and R. A. Athale, "Computational imaging," Advances in Optics and Photonics, 10(2), 409-483, 2018.

[6] G. Lipworth et al., "Comprehensive simulation platform for a metamaterial imaging system," Applied optics, 54(31), 9343-9353.

[7] R. Sharma, O. Yurduseven, B. Deka, and V. Fusco, "Hardware Enabled Acceleration of Near-Field Coded Aperture Radar Physical Model for Millimetre-Wave Computational Imaging," Progress In Electromagnetics Research B, 90, 91-108, 2021.

[8] S. S. Ahmed, Electronic microwave imaging with planar multistatic arrays. Logos Verlag Berlin GmbH, 2014.

[9] S. S. Ahmed et al., "Advanced microwave imaging," IEEE microwave magazine, 13(6), 26-43, 2012.

[10] G. R. Lockwood, P. C. Li, M. O'Donnell, and F. S. Foster, "Optimizing the radiation pattern of sparse periodic linear arrays," IEEE Transactions on Ultrasonics, Ferroelectrics, and frequency control, 43(1), 7-14, 1996.

[11] W. F. Moulder et al., "Development of a high-throughput microwave imaging system for concealed weapons detection," In 2016 IEEE International Symposium on Phased Array Systems and Technology (PAST) (pp. 1-6). IEEE, October 2016.

[12] Z. Wang et al., "Near-field 3-D millimeter-wave imaging using MIMO RMA with range compensation," IEEE Transactions On Microwave Theory and Techniques, 67(3), 1157-1166, 2018.

[13] Y. Ding, and D. J. Munson, "A fast back-projection algorithm for bistatic SAR imaging," In Proceedings. International Conference on Image Processing (Vol. 2, pp. II-II). IEEE, September 2002.

[14] T. Sleasman et al., "Single-frequency microwave imaging with dynamic metasurface apertures," JOSA B, 34(8), 1713-1726, 2017.

[15] H. Odabasi et al., "Investigation of alignment errors on multi-static microwave imaging based on frequency-diverse metamaterial apertures," Progress In Electromagnetics Research B, 70, 101-112, 2016.